catalysts

MDPI

Article

Mineralization of Riluzole by Heterogeneous Fenton Oxidation Using Natural Iron Catalysts

Nasr Bensalah [1,*], Emna Neily [2], Ahmed Bedoui [2] and Mohammad I. Ahmad [3,*]

[1] Program of Chemistry, Department of Chemistry and Earth Sciences, College of Arts and Science, Qatar University, Doha P.O. Box 2713, Qatar
[2] Department of Chemistry, Faculty of Sciences of Gabes, University of Gabes, Gabes 6072, Tunisia
[3] Central Laboratories Unit, Qatar University, Doha P.O. Box 2713, Qatar
* Correspondence: nasr.bensalah@qu.edu.qa (N.B.); mohammad.ibrahim@qu.edu.qa (M.I.A.)

Abstract: Fenton (H_2O_2/Fe^{2+}) system is a simple and efficient advanced oxidation technology (AOT) for the treatment of organic micropollutants in water and soil. However, it suffers from some drawbacks including high amount of the catalyst, acid pH requirement, sludge formation and slow regeneration of Fe^{2+} ions. If these drawbacks are surmounted, Fenton system can be the best choice AOT for the removal of persistent organics from water and soil. In this work, it was attempted to replace the homogeneous catalyst with a heterogeneous natural iron-based catalyst for the decomposition of H_2O_2 into oxidative radical species, mainly hydroxyl ($HO^{\bullet}$) and hydroperoxyl radicals ($HO_2^{\bullet}$). The natural iron-based catalyst is hematite-rich (α-Fe_2O_3) and contains a nonnegligible amount of magnetite (Fe_3O_4) indicating the coexistence of Fe (III) and Fe(II) species. A pseudo-first order kinetics was determined for the decomposition of H_2O_2 by the iron-based solid catalyst with a rate constant increasing with the catalyst dose. The catalytic decomposition of H_2O_2 into hydroxyl radicals in the presence of the natural Fe-based catalyst was confirmed by the hydroxylation of benzoic acid into salicylic acid. The natural Fe-based catalyst/H_2O_2 system was applied for the degradation of riluzole in water. It was demonstrated that the smaller the particle size of the catalyst, the larger its surface area and the greater its catalytic activity towards H_2O_2 decomposition into hydroxyl radicals. The degradation of riluzole can occur at all pH levels in the range 3.0–12.0 with a rate and efficiency greater than H_2O_2 oxidation alone, indicating that the natural Fe-based catalyst can function at any pH without the need to control the pH by the addition of chemicals. An improvement in the efficiency and kinetics of the degradation of riluzole was observed under UV irradiation for both homogeneous and heterogeneous Fenton systems. The results chromatography analysis demonstrate that the degradation of riluzole starts by the opening of the triazole ring by releasing nitrate, sulfate, and fluoride ions. The reuse of the catalyst after heat treatment at 500 °C demonstrated that the heat-treated catalyst retained an efficiency >90% after five cycles. The results confirmed that the natural sources of iron, as a heterogeneous catalyst in a Fenton-like system, is an appropriate replacement of a Fe^{2+} homogeneous catalyst. The reuse of the heterogeneous catalyst after a heat-treatment represents an additional advantage of using a natural iron-based catalyst in Fenton-like systems.

Keywords: Fenton system; natural iron-based catalyst; hydroxyl radicals; riluzole; degradation

Citation: Bensalah, N.; Neily, E.; Bedoui, A.; Ahmad, M.I. Mineralization of Riluzole by Heterogeneous Fenton Oxidation Using Natural Iron Catalysts. *Catalysts* **2023**, *13*, 68. https://doi.org/10.3390/catal13010068

Academic Editor: Victorio Cadierno

Received: 13 May 2022
Revised: 14 September 2022
Accepted: 23 September 2022
Published: 30 December 2022

1. Introduction

Natural waters including surface and ground waters are less than 3% of the global water on the Earth, but they represent 98% of human consumption. Nowadays, there is extensive demand for natural water resources due to exponential population growth, expanded anthropogenic activities, and massive urbanization [1,2]. These result in the discharge of substances and the extraction of resources, thereby increasing the pollution of the environment. Water, being partially responsible for the cycling of elements within

the global biogeochemical cycle, has been the most affected part of the environment and a diversity of organic pollutants are transferred to the ground and surface waters [3,4]. The contamination of these natural waters with anthropogenic organic micropollutants from diverse sources causes economic, health, and environmental problems [5–8]. Conventional biological treatment methods fail to remove the anthropogenic organic micropollutants from water [9]. Therefore, an urgent development of water treatment technologies is essential to cope with the (re)use of the valuable natural water resources.

Advanced oxidation technologies (AOTs) are among the most effective technologies in eliminating organic micropollutants from water through their mineralization into CO_2, H_2O, and inorganic ions [10–13]. AOTs are based on the production of oxidizing radical species, mainly hydroxyl radicals ($HO^{\bullet}$), by redox reactions between reducing and oxidizing reagents and/or by the combination of chemical oxidants with activating methods [13–15]. The $HO^{\bullet}$ radicals are potent and instable oxidants capable of reacting non-selectively with organic micropollutants and transforming them into less harmful intermediates that end by being mineralized. Fenton oxidation method is an inexpensive advanced oxidation technology that is simple to implement in water treatment plants. Fenton oxidation utilizes ferrous iron as a homogeneous catalyst to decompose hydrogen peroxide (H_2O_2) in acid medium into radical species, including hydroxyl radicals ($HO^{\bullet}$) and hydroperoxyl radicals ($HO_2^{\bullet}$) (Equations (1)–(7)) [13,16–19].

$$Fe^{2+} + H_2O_2 \rightarrow Fe^{3+} + HO^{\bullet} + OH^{-} \quad (1)$$

$$Fe^{2+} + HO^{\bullet} \rightarrow Fe^{3+} + OH^{-} \quad (2)$$

$$Fe^{3+} + H_2O_2 \rightarrow Fe\text{-}OOH^{2+} + H^{+} \quad (3)$$

$$Fe\text{-}OOH^{2+} \rightarrow Fe^{2+} + HO_2^{\bullet} \quad (4)$$

$$Fe^{2+} + HO_2^{\bullet} \rightarrow Fe^{3+} + HO_2^{-} \quad (5)$$

$$Fe^{3+} + HO_2^{\bullet} \rightarrow Fe^{2+} + O_2 + H^{+} \quad (6)$$

$$H_2O_2 + HO^{\bullet} \rightarrow HO_2^{\bullet} + H_2O \quad (7)$$

The rate-determining step in the Fenton oxidation method is the regeneration of the Fe^{2+} homogeneous catalyst. This step is rendered slow and incomplete due to several factors, including the precipitation of Fe^{3+} as iron(III) hydroxide at mild acid or neutral pH, and rapid reactions of Fe^{2+} with $HO^{\bullet}$ and $HO_2^{\bullet}$ radicals (Equations (2) and (5)). For effective and continuous production of $HO^{\bullet}$ and $HO_2^{\bullet}$ radicals, large amounts of Fe^{2+} catalyst are needed, which poses a secondary pollution and needs a post-treatment stage to neutralize the treated wastewater and separate the residual ferric hydroxide sludge. The recycling of the iron sludge is not practical. Furthermore, a careful control of the catalyst dose and H_2O_2 concentration is important to limit the scavenging reactions (Equations (2), (5) and (7)) and keep high efficiency for Fenton oxidation towards the degradation of the organic micropollutants [20–24].

Heterogeneous Fenton-like systems using natural sources of iron can be a good solution to overcome the drawbacks of a homogeneous Fenton system, including large amounts of chemicals, the slow regeneration of the catalyst, and sludge post-treatment. Minerals and ores rich in iron such as magnetite (Fe_3O_4) [25], maghemite (γ-Fe_2O_3) [26,27], hematite (α-Fe_2O_3) [28,29] and pyrite (FeS_2) [30,31] are examples of naturally occurring heterogeneous Fenton-like catalysts for the degradation of micropollutants in water. In a heterogeneous Fenton-like system, the typical mechanism of degradation involves the adsorption of micropollutant molecules on the surface of the solid catalyst, the dissociation of H_2O_2 on the surface of the catalyst into radical species ($HO^{\bullet}$ and $HO_2^{\bullet}$), and the immediate attack of $HO^{\bullet}$ and $HO_2^{\bullet}$ radicals on the adsorbed micropollutant molecules [32–34]. The natural heterogeneous Fenton-like systems can attain complete mineralization of organic micropollutants at different pH conditions with lower cost than a homogeneous Fenton system [35–37].

In this work, a natural iron source catalyst rich in hematite was extracted from a mining site in northern Tunisia and used in the degradation of riluzole as a model of bioresistant organic micropollutants in water (see chemical structure). The decomposition of H_2O_2 in radical species using the natural iron-based heterogeneous catalyst was investigated. The effects of certain experimental parameters, including the catalyst dose and particle size, the initial pH, H_2O_2 concentration, and UV irradiation on the efficiency of riluzole degradation using the heterogeneous Fenton system (iron-based catalyst/H_2O_2) were evaluated. The results of riluzole degradation by heat and acid-treated heterogeneous and homogeneous catalysts were also compared. Furthermore, the leaching of iron ions from the natural Fe-based catalyst at different pH levels was studied in order to evaluate the feasibility of the heterogeneous Fenton-like system proposed herein.

2. Results and Discussion

2.1. Characterization of Natural Fe-Based Catalyst

The XRD spectrum of the rusty red natural Fe-based ore shows the predominance of hematite Fe_2O_3 phase with the presence of impurities of magnetite Fe_3O_4 as indexed in Figure 1a. The XRD pattern coincides with the rhombohedral α-Fe_2O_3 crystalline structure (JCPDS# 33-0664) [28].

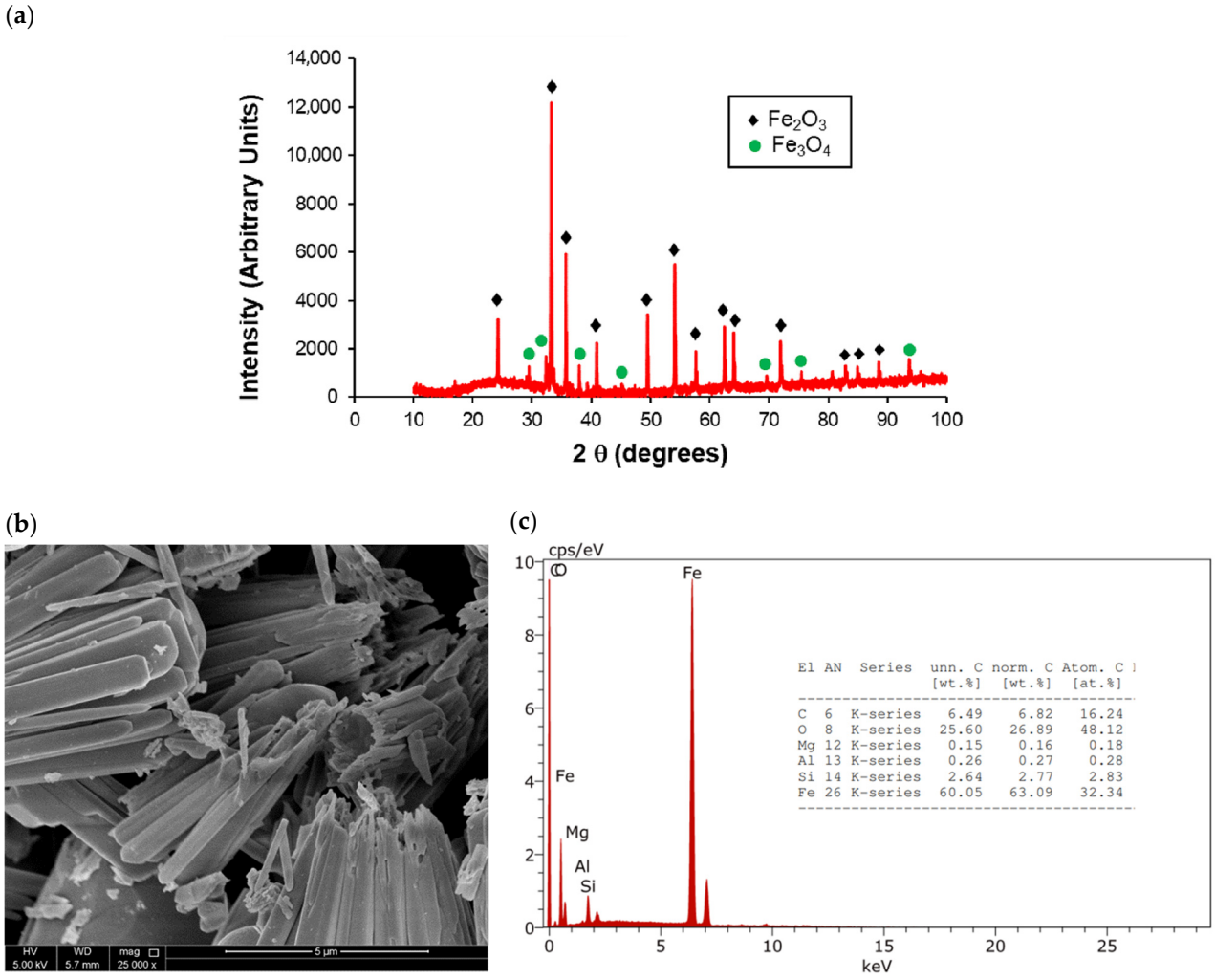

Figure 1. (**a**) XRD spectrum, (**b**) SEM image, and (**c**) EDS spectrum of the natural Fe-based catalyst.

The SEM image of Figure 1b demonstrates a homogeneous morphology with stacked micro-rods having a 0.2–0.5 µm diameter and a 3–5 µm length. The SEM-EDS spectrum of Figure 1c confirms the presence of Fe (~63.1% wt.) and O (~26.9% wt.), C (~6.8% wt.),

Mg (~0.15% wt.), Al (~0.3% wt.), and Si (~2.8% wt.) elements. The O:Fe molar ratio was between 1.45 and 1.48 measured at different surface locations. This is in accordance with the XRD spectrum showing the presence of Fe_3O_4 impurities in addition to Fe_2O_3, which corroborates the value of the O:Fe molar ratio being less than 1.5. The composition of this natural Fe-based ore extracted from northern Tunisia confirms that it is rich in Fe (63.1% wt.) and indicates that Fe(III) is the predominant Fe form. Similar results were reported in literature for natural iron ores in different regions in the world [27,38,39].

2.2. Decomposition of H_2O_2 by Natural Fe-Based Heterogeneous Catalyst

The finely grinded natural Fe-based ore was tested as a heterogeneous Fenton catalyst for the decomposition of H_2O_2 into hydroxyl radicals. Figure 2a shows the changes of H_2O_2 concentration with time during its reaction with different doses of Fe-based catalyst. H_2O_2 concentration declines exponentially with time in the presence of a Fe-based catalyst, indicating a pseudo-first order kinetics for the decomposition of H_2O_2 (Figure 2a). The increase of the catalyst dose increases the rate constant of the decomposition of H_2O_2 as shown in Figure 2a (inlet). The catalytic decomposition of H_2O_2 into hydroxyl radicals in the presence of the natural Fe-based catalyst was confirmed by the hydroxylation of benzoic acid (122 ppm) into salicylic acid (Figure 2b,c). Figure 2c demonstrates the increase of salicylic acid concentration with time for all the catalyst doses, confirming the hydroxylation of benzoic acid. An increase in the Fe-based catalyst dose increases the maximum concentration of salicylic acid formed during 60 min. The average rate of the formation of salicylic acid within the first 20 min increases linearly with the Fe-based catalyst dose (Figure 2d). The higher the dose of the Fe-based catalyst, the more rapid is the formation/disappearance of salicylic acid during the oxidation of benzoic acid by the H_2O_2/Fe-based catalyst system.

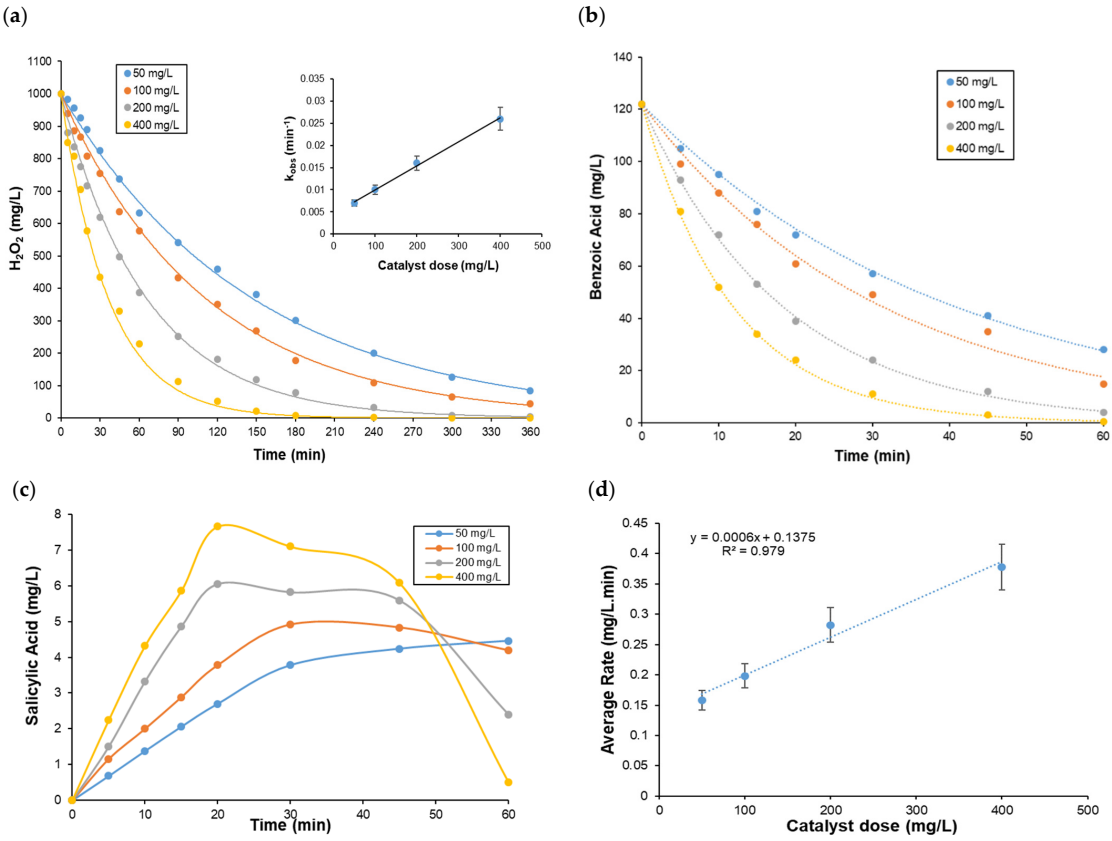

Figure 2. (**a**) Kinetics of the decomposition of H_2O_2 (1000 mg/L) with a Fe-based catalyst. Inlet: Increase of pseudo-first order rate constant with catalyst dose (50–400 mg/L, (particle size < 200 µm); (**b**) Degradation of benzoic acid, (exponential trend lines are added to graphs a and b); (**c**) Formation

of salicylic acid, and (**d**) Dependence of the average rate of formation of salicylic acid on the catalyst dose during the degradation of benzoic acid (122 mg/L) using a H_2O_2 (1000 mg/L)/Fe-based catalyst (50–400 mg/L, particle size < 200 µm) system. Experimental conditions: pH = 3.0, Temperature: 23–25 °C, Mixing rate: 400 rpm.

These results indicate that H_2O_2 decomposition by the heterogeneous natural Fe-based catalyst leads to the formation of hydroxyl radicals by the Fenton-like reaction. These hydroxyl radicals immediately attack benzoic acid to form salicylic acid as an intermediate that undergoes oxidation with hydroxyl radicals, and its concentration rapidly declines. Larger production of hydroxyl radicals is observed in the presence of higher natural Fe-based catalyst doses. These results confirm that the natural Fe-based ore can be used as a heterogeneous catalyst for the decomposition of H_2O_2 into hydroxyl radicals in a Fenton-like process [32,33].

2.3. Degradation of Riluzole by H_2O_2/Fe-Based Catalyst Heterogeneous Fenton System

The results of the treatment of 23.4 mg/L (~0.1 mM) riluzole aqueous solutions using an Fe-based catalyst alone, H_2O_2 alone, an Fe-based catalyst/H_2O_2 (heterogeneous Fenton system) and Fe^{2+}/H_2O_2 (homogeneous Fenton system) at pH = 3.0 and room temperature (23–25 °C) are presented in Figure 3. The adsorption on the surface of Fe-based catalyst cannot remove more than 8% of riluzole from water at the end of the treatment due to the saturation of the active sites of the catalyst. H_2O_2 oxidation alone accomplished 16.7% riluzole removal from water. The combined system Fe-based catalyst/H_2O_2, known as the Fenton-like system, achieved a complete riluzole removal from the water within 360 min. The complete riluzole removal was obtained by the homogeneous Fenton system (Fe^{2+}/H_2O_2) within a shorter time (300 min) than the heterogeneous Fenton system. The concentration of riluzole declined exponentially with time with H_2O_2 oxidation and the combined systems Fe-based catalyst/H_2O_2 and (Fe^{2+}/H_2O_2), indicating a pseudo-first order kinetics for riluzole degradation (see Figure 3). The pseudo-first order rate constants 5.0×10^{-4} min^{-1}, 2.0×10^{-2} min^{-1}, and 3.0×10^{-2} min^{-1} were calculated for H_2O_2 oxidation, Fe-based catalyst/H_2O_2, and (Fe^{2+}/H_2O_2), respectively. This demonstrates the higher efficiency of the combined systems than the single ones owing to the production of hydroxyl radicals by Fenton reaction in solution or at the surface of the Fe-based catalyst. These strong and powerful oxidizing radical species react immediately with the organic molecules of riluzole and decline riluzole concentration in solution. Although the kinetics of riluzole degradation by a homogeneous Fenton system is better than by a heterogeneous Fenton system, the utilization of natural sources of Fe-based catalyst in Fenton oxidation is highly important for scalable applications due to the lower costs, less sludge waste, and the recyclability of the heterogeneous catalyst [33,40].

Figure 4 presents the effect of Fe-based catalyst particle size on the kinetics of riluzole (23.4 mg/L) degradation by a Fe-based catalyst/H_2O_2 system. The results showed an important effect of the particle size of the solid catalyst on the kinetics of riluzole degradation. Pseudo-first order kinetics were observed for all the particle sizes tested (Figure 4a); however, the pseudo-first order rate constant decreases with the increase of the catalyst particle size (Figure 4b). The highest rate constant of 2×10^{-2} min^{-1} was calculated for particle size less than 200 µm; while the smallest rate constant of 8×10^{-3} min^{-1} was measured for particle size greater than 1000 µm. Rate constants of 1.3×10^{-2} min^{-1} and 1.0×10^{-2} min^{-1} were found for particle size between 200 and 500 µm and between 500 and 1000 µm, respectively; the smaller the particle size of the catalyst, the larger its surface area. A larger surface area has more active sites to catalyze the decomposition of H_2O_2 into hydroxyl radicals and to adsorb riluzole molecules, which are reasons to explain the more rapid and highly efficient degradation of riluzole for particle size less than 200 µm of the natural Fe-based catalyst.

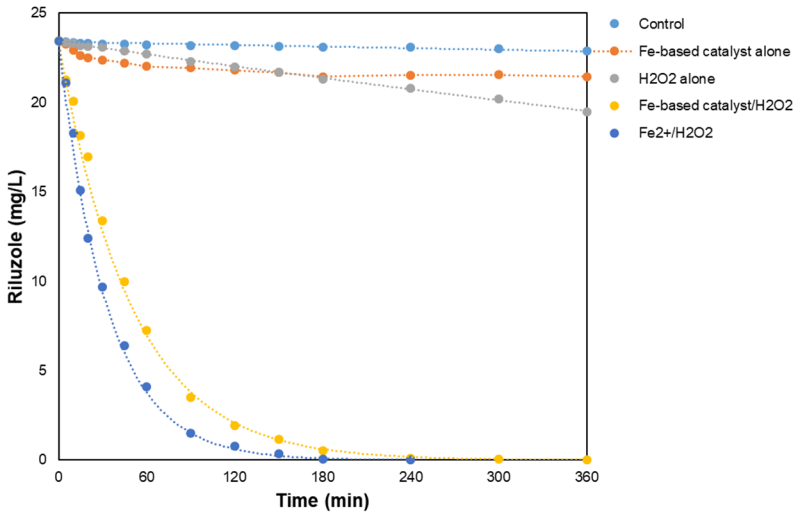

Figure 3. Changes of riluzole concentration with time during the treatment of 23.4 mg/L riluzole aqueous solutions using a Fe-based catalyst/H_2O_2 system (exponential trend lines are added dashed lines). Experimental conditions: H_2O_2: 1000 mg/L, Fe-based catalyst: 200 mg/L (particle size < 200 µm), Fe^{2+}: 140 mg/L, pH = 3.0, Temperature: 23–25 °C, Mixing rate: 400 rpm.

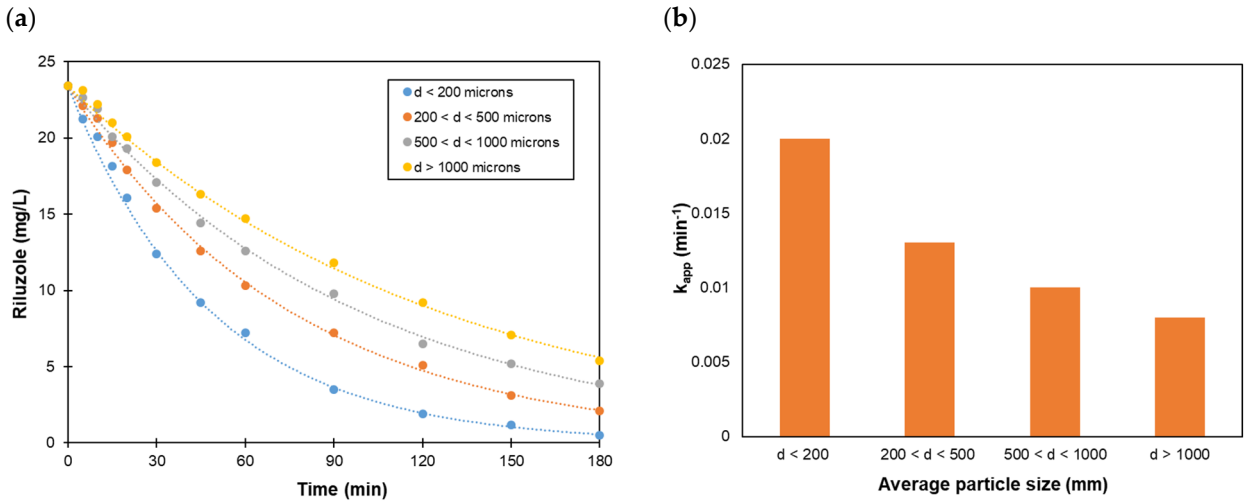

Figure 4. Effect of Fe-based catalyst particle size on (**a**) the changes of riluzole concentration with time and (**b**) the pseudo-first order rate constant during the treatment of 23.4 mg/L riluzole aqueous solutions using Fe-based catalyst/H_2O_2 system (exponential trend lines are added to graphs in dashed lines). Experimental conditions: H_2O_2: 1000 mg/L, Fe-based catalyst: 200 mg/L, pH = 3.0, Temperature: 23–25 °C, Mixing rate: 400 rpm.

The results of the effect of pH on the kinetics and efficiency of the degradation of riluzole by a Fe-based catalyst/H_2O_2 system are presented in Figure 5a,b. Almost complete removal of riluzole was obtained at pH 3.0 and 5.0 within 360 min (Figure 5a); while only 92.3%, 84.5%, and 65.0 of riluzole were removed after 360 min at pH 7.0, 9.0, and 12.0, respectively. The pseudo-first order rate constant of riluzole degradation decreased with the increase of pH from 3.0 to 12.0 as shown in Figure 5b. It is well reported that the degradation of organic pollutants by homogeneous Fenton (Fe^{2+}/H_2O_2) system is efficient under acid conditions (pH in the range 3.0–4.0) [40,41]. Compared to a homogeneous Fenton system (Fe^{2+}/H_2O_2), in which the rate constant of degradation of riluzole decreased abruptly with the increase of pH (the rate constant was equal to H_2O_2 oxidation alone for pH 7.0, 9.0, and 12.0), the decrease in rate constant with the pH for a heterogeneous Fenton system (Fe-based catalyst/H_2O_2) was decelerated when pH increased. However,

the degradation of riluzole occurred at all pH levels in the range 3.0–12.0 with a rate and efficiency greater than H_2O_2 oxidation alone. This result is very important in real applications where the pH of wastewaters is usually in the range between 4.0 to 8.5; the natural Fe-based catalyst can function in this range and does not necessitate the control of the pH by the addition of chemicals.

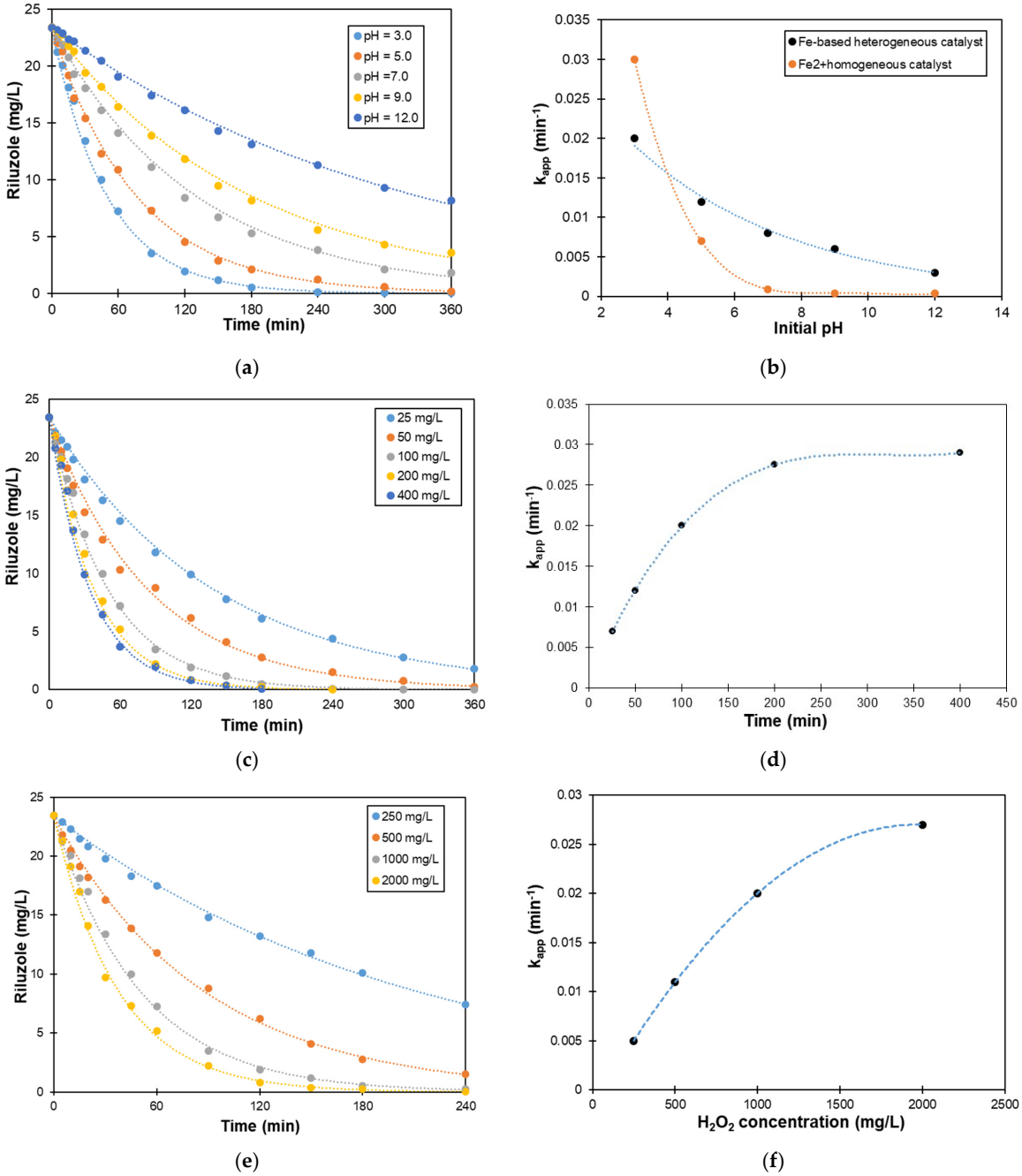

Figure 5. (**a**,**b**) Effect of initial pH (H_2O_2: 1000 mg/L, Fe-based catalyst: 200 mg/L (particle size < 200 μm), pH: 3.0–12.0), (**c**,**d**) Effect of catalyst dose (H_2O_2: 1000 mg/L, Fe-based catalyst: 25–400 mg/L (particle size < 200 μm), pH = 3.0), and (**e**,**f**) Effect of H_2O_2 concentration (H_2O_2: 250–2000 mg/L, Fe-based catalyst: 200 mg/L (particle size < 200 μm), pH = 3.0) on the changes of riluzole concentration with time and on the first-order rate constant during the treatment of 23.4 mg/L riluzole aqueous solutions using a Fe-based catalyst/H_2O_2 system at T = 23–25 °C and under 400 rpm mixing rate. (Exponential trend lines are added to graphs a, c, and e in dashed lines).

The results of the effect of the catalyst dose on the degradation of riluzole (23.4 mg/L) by a Fe-based catalyst/H_2O_2 system are presented in Figure 5c,d. The increase of the catalyst dose from 50 mg/L to 200 mg/L enhanced the efficiency of riluzole degradation (Figure 5c) after 360 min from 92% to 98.9, and 100% for catalyst doses of 50, 100, and 200 mg/L. Figure 5d shows that the first-order rate constant increases linearly with the catalyst dose up to 200 mg/L. This result can be explained by the increase of catalytic active sites of the heterogeneous catalyst and then the larger production of hydroxyl radicals. However, further increase in the catalyst dose to doses higher than 200 mg/L did not show a significant improvement in the efficiency and kinetics of riluzole degradation (The rate constant was maintained to the same value as that of 200 mg/L). Doses of the heterogeneous catalyst higher than 200 mg/L seem to be less effective due to the competition of riluzole oxidation with secondary reactions in consuming excessive amounts of hydroxyl radicals (including surface oxidation of Fe^{2+}, reaction with H_2O_2, combination to form H_2O_2). It is clear that a catalyst dose of 200 mg/L is optimal and sufficient to completely remove riluzole from the water. In a similar way, the increase of H_2O_2 concentration from 250 to 2000 mg/L increased the efficiency of riluzole degradation after 240 min from 88.0% to 96.6%, 99.7%, and 99.9% for 250, 500, 1000, and 2000 mg/L, respectively. The first-order rate constant increased with the increase of H_2O_2 concentration with higher ramp for H_2O_2 concentrations lower than 1000 mg/L (Figure 5f). H_2O_2 concentrations higher than 1000 mg/L did not lead to an important enhancement in the efficiency and kinetics of riluzole degradation considering the cost increment by using high H_2O_2 amounts. The increase in H_2O_2 concentration up to 1000 mg/L enlarges the production of hydroxyl radicals, which enhances the kinetics and efficiency of riluzole degradation. However, the excessive formation of hydroxyl radicals formed at H_2O_2 concentration higher than 1000 mg/L seems to be unwholesome (not beneficial) to the degradation of riluzole because of their non-selective reaction with organic and inorganic components in solution and on the surface of the catalyst. An H_2O_2 concentration of 1000 mg/L was selected as an optimal concentration for a cost-effective degradation of riluzole.

The effect of UV light irradiation on the degradation of riluzole (23.4 mg/L) by a Fe-based catalyst/H_2O_2 system was also studied under the optimal conditions of pH (pH = 3.0), catalyst dose (200 mg/L), and H_2O_2 concentration (1000 mg/L). An improvement in the efficiency and kinetics of the degradation of riluzole was obtained under UV irradiation for both homogeneous and heterogeneous Fenton systems as shown in Figure 6a. All the Fenton and photo-assisted Fenton systems achieved the complete removal of riluzole after different periods: 300 min for Fe-based catalyst/H_2O_2, 240 min for Fe^{2+}/H_2O_2, 120 min for Fe-based catalyst/H_2O_2/UV, and 90 min for Fe^{2+}/H_2O_2/UV. Figure 6b presents the changes of TOC with time for homogeneous and heterogeneous Fenton and photo-assisted Fenton systems during the treatment of 23.4 mg/L aqueous solutions. TOC content declines exponentially with time for all the systems except for H_2O_2 oxidation alone where TOC remains almost constant. The TOC removal at the end of the treatment (after 360 min) were 55.8%, 69.2%, 88.4%, and 92.3% for Fe-based catalyst/H_2O_2, Fe^{2+}/H_2O_2, Fe-based catalyst/H_2O_2/UV, and Fe^{2+}/H_2O_2/UV, respectively.

The pseudo-first order rate constants calculated for TOC were 0.002, 0.003, 0.006, and 0.007 min^{-1} for Fe-based catalyst/H_2O_2, Fe^{2+}/H_2O_2, Fe-based catalyst/H_2O_2/UV, and Fe^{2+}/H_2O_2/UV, respectively. It can be concluded that the effect of UV irradiation is more profound on the kinetics and efficiency of TOC removal. UV irradiation enhances TOC removal for homogeneous and heterogeneous Fenton systems due to the production of supplementary hydroxyl radicals by homolytic photo-dissociation of H_2O_2 and rapid regeneration of the catalytic active sites by photodecomposition of iron-carboxylate complexes.

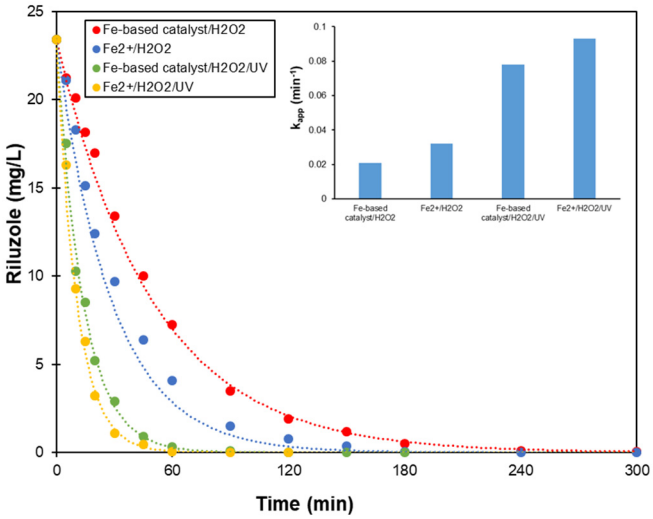

(**a**)

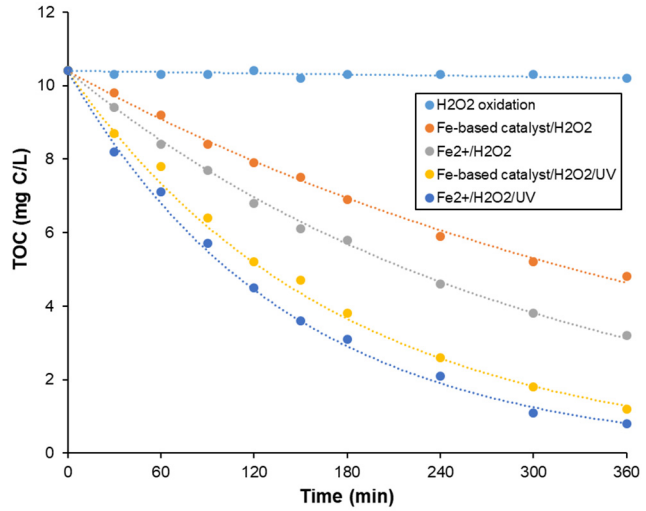

(**b**)

Figure 6. Effect of UV irradiation on the changes of (**a**) riluzole concentration, and (**b**) TOC content during the treatment of 23.4 mg/L riluzole aqueous solutions by homogeneous and heterogeneous Fenton and photo-assisted Fenton systems. Experimental conditions: H_2O_2: 1000 mg/L, Fe-based catalyst: 200 mg/L (particle size < 200 μm), Fe^{2+}: 140 mg/L, UV irradiation: Medium mercury pressure lamp (Light wavelength range: 200–600 nm, power input: 150 W), pH = 3.0, Temperature: 23–25 °C, Mixing rate: 400 rpm.

Leaching of iron ions from the natural Fe-based catalyst is an important factor in determining its future utilization for real cases. Figure 7a presents the changes of the concentration of dissolved iron with time at different pH in the range between 3.0 and 12.0. The concentration of dissolved iron increases with time for all the pH media. Higher concentrations of dissolved iron were measured at pH 12.0 and 3.0, while the lowest concentration of dissolved iron was measured at pH = 7.0. The final concentrations of dissolved iron measured at all pH values were less than 5 mg/L (<4% of the total iron contained in the catalyst composition), indicating low leaching properties of the natural Fe-based catalyst. The amount of dissolved iron does not pose an environmental problem for the discharge of treated wastewater.

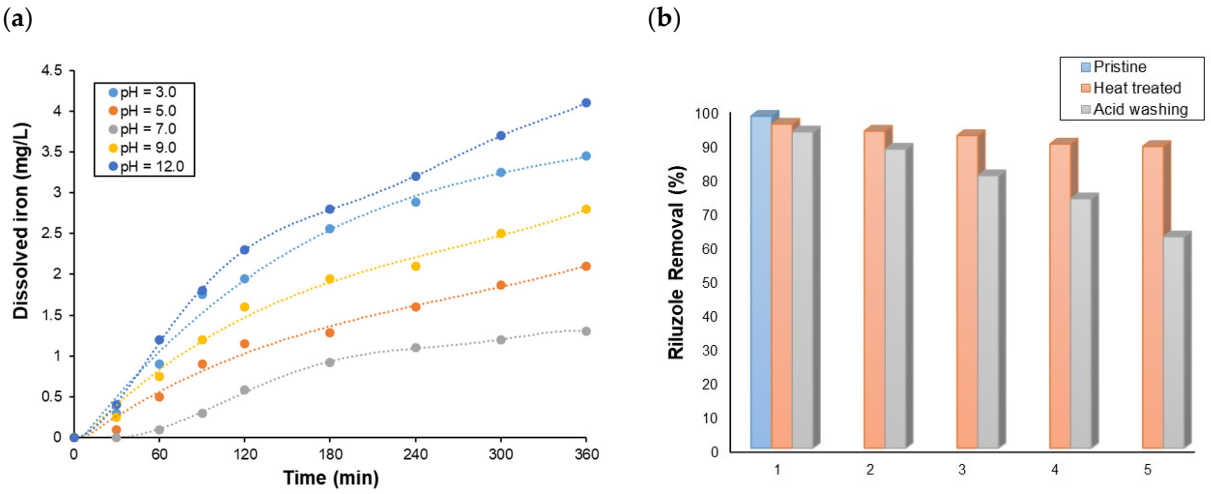

Figure 7. (**a**) Changes of dissolved iron with time at different pH values, (**b**) riluzole removal yield using pristine, heat-treated, and acid-washed catalyst after cycles 1–5 at pH 3.0 during the treatment of 23.4 mg/L riluzole aqueous solutions by Fe-based catalyst/H_2O_2. Experimental conditions: H_2O_2: 1000 mg/L, Fe-based catalyst: 200 mg/L (particle size < 200 µm), Temperature: 23–25 °C, Mixing rate: 400 rpm.

The reuse of the catalyst after heat treatment at 500 °C for 120 min and acid washing was evaluated for the treatment of 23.4 mg/L riluzole aqueous solutions using a Fe-based catalyst/H_2O_2. Figure 7b presents the riluzole removal yield for pristine catalyst, heat-treated catalyst, and acid-washed catalyst after five consecutive cycles. The heat-treated catalyst retained an excellent efficiency (>90%) in removing riluzole from the water after five cycles. However, the efficiency of the acid-treated catalyst dropped from one cycle to another to reach 62.4% after five cycles. This result indicates that heat treatment at 500 °C can be chosen for the reuse of the natural Fe-based catalyst in Fenton-like systems to treat wastewaters contaminated with organic pollution. The potential reuse of the Fe-based-catalyst will contribute to the reduction of the total cost of wastewater treatment. The promising results of a Fe-based catalyst/H_2O_2 heterogeneous Fenton system in the degradation of riluzole (as a model of organic pollution in water) indicate the potential implementation of this natural catalyst due to its high stability and its reusability after heat-treatment activation.

2.4. Proposed Mechanism of Riluzole Degradation of by Fe-Based Catalyst/H_2O_2 System

The changes of riluzole concentration, intermediates concentration, and TOC content (all expressed in mg C/L) with time during the treatment of 23.4 mg/L riluzole aqueous solutions using Fe-based catalyst/H_2O_2 system under the optimal conditions of pH (pH = 3.0), catalyst dose (200 mg/L), and H_2O_2 concentration (1000 mg/L) are presented in Figure 8a. The decline of riluzole with time is tenfold more rapid than TOC, and it is accompanied by a rapid formation of aromatic and aliphatic intermediates. The decrease of TOC content indicates the mineralization of organic carbon and release of CO_2 as final product. The concentration of the intermediates reaches a maximum of 7.1 mg C/L between 120 and 150 min, and then it start to decay with the same rate as TOC until the end of the treatment. The total concentration of C4 carboxylic acids (fumaric and maleic acids) increases from the beginning of the treatment to reach a maximum of 2.5 mg C/L after 120 min, and then their total concentration decreases, and they finish by being removed totally from the water after 300 min. However, the concentration of C2 carboxylic acids (oxalic and acetic acids) starts to rise after 60 min and reaches a plateau after 180 min, indicating the accumulation of C2 carboxylic acids that persists until the end of the treatment. The estimated concentration of aromatic intermediates (calculated from the following mass balance equation: Total intermediates = Aromatic intermediates + C4 carboxylic acids + C2 carboxylic acids)

increases rapidly from the beginning of the treatment to reach a maximum of 4.9 mg C/L after 60 min and then declines quickly to disappear completely after 180 min. HPLC analysis demonstrates the formation of 4-(trifluoromethoxy) aniline (4-TFMA), aniline, and 4-aminophenol as aromatic intermediates among others (Figure 8b). The concentrations of the three intermediates increase rapidly with time to reach a maximum after 60–90 min, and then they decline to zero after 180 min.

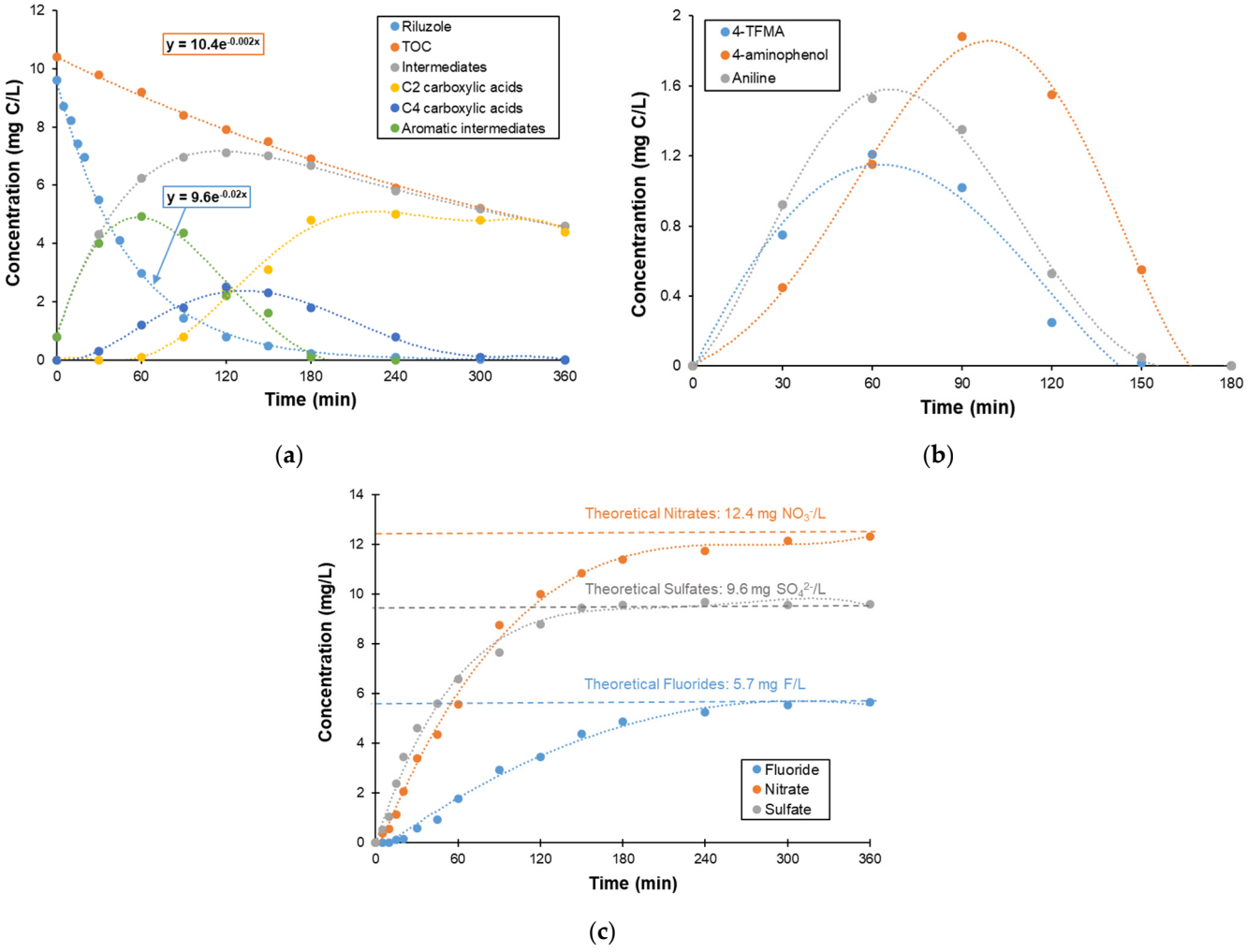

Figure 8. Changes of the concentrations of (**a**,**b**) organic intermediates, and (**c**) inorganic ions during the treatment of 23.4 mg/L riluzole aqueous solutions by homogeneous and heterogeneous Fenton and photo-assisted Fenton systems. Experimental conditions: H_2O_2: 1000 mg/L, Fe-based catalyst: 200 mg/L (particle size < 200 µm), pH = 3.0, Temperature: 23–25 °C, Mixing rate: 400 rpm.

Figure 8c presents the changes of the concentrations of inorganic ions (fluorides, sulfates, and nitrates) with time during the treatment of 23.4 mg/L riluzole aqueous solutions using a Fe-based catalyst/H_2O_2 system under the optimal conditions of pH (pH = 3.0), catalyst dose (200 mg/L), and H_2O_2 concentration (1000 mg/L). The concentrations of fluorides, sulfates, and nitrates increase linearly with time, and then they reach plateaus at the end of the treatment. The plateaus coincide with the theoretical concentrations of fluorides, sulfates, and nitrates contained initially in 23.4 mg/L riluzole aqueous solutions. This result demonstrates the complete release of organic fluorine, sulfur, and nitrogen in the form of fluorides, sulfates, and nitrates, respectively. The average rates of release of sulfates, nitrates, and fluorides (slopes of the linear tails) within the first 60 min were estimated to be 0.124, 0.096, and 0.024 mg/L.min, respectively. This indicates that the release of fluoride is slower than nitrates and sulfates. Based on these results, a simple mechanism

was proposed for the degradation of riluzole. The degradation of riluzole starts by the opening of the triazole ring to form aromatic derivatives including 4-TFMA, aniline, and 4-aminophenol releasing nitrate, sulfate, and fluoride ions. An oxidative opening of the benzene ring forms C4 carboxylic acids that are quickly fragmented into C2 carboxylic acids. C2 carboxylic acids are slowly oxidized into CO_2 and H_2O.

3. Materials and Methods

3.1. Chemicals

Riluzole (2-Amino-6-(trifluoromethoxy)benzothiazole), 4-(trifluoromethoxy) aniline, aniline, and 4-aminophenol were purchased from Sigma-Aldrich. Iron(II) sulfate heptahydrate ($FeSO_4$. $7H_2O$), sulfuric acid (H_2SO_4), sodium hydroxide (NaOH), sodium sulfite (Na_2SO_3), 30% hydrogen peroxide (H_2O_2) were bought from VWR in high-purity grade. The other substances used in chromatography analysis were analytical grade Fluka (Buchs, Switzerland) chemicals. The synthetic solutions were prepared using deionized water received from a Millipore Milli-Q system having a resistivity >18 MΩ cm^{-1} at 25 °C.

3.2. Analytical Methods

The measurement of the total organic carbon (TOC) was measured using Skalar Formacs^{HT} TOC/TN analyzer. The analysis of inorganic ions (fluoride, sulfate, and nitrate) was carried out using a Dionex ICS-2000 ion chromatograph equipped with IonPac AG19 guard column (4 × 50 mm), IonPac AS19 separation column (4 × 250 mm), and (EGC), ASRS 300-4 mm suppressor, DS6 conductivity cell, and AS auto-sampler. A total of 20 mM aqueous solution of potassium hydroxide (KOH) supplied by the eluent generator was used as mobile phase was at a constant 1mL/min flow rate. Standard solutions of sulfate, fluoride, and nitrate were prepared by dilution of stock solutions to concentrations ranging from 0.1 mg/L to 20 mg/L. Linear calibration curves were plotted with correlation coefficients (R^2) higher than 0.99. The analysis of riluzole and its aromatic degradation products was performed using reversed phase chromatography by a HPLC-UV (Agilent 1100 series) chromatograph equipped with Phenomenex Gemini 5 µm C18 at a constant [42]. The detection UV wavelength was fixed at 260 nm, and the column temperature was maintained at 25 °C. The mobile phased is composed of a mixture of solvent A (25 mM of formic acid aqueous solution) and Solvent B (acetonitrile). A lineal gradient chromatographic elution was adopted by initially running 10% of Solvent B, ascending to 100% in 40 min. Before analysis, the withdrawn samples of treated solutions were filtered using 0.45 µm membrane filters. Inductively coupled plasma-optical emission spectrometer (ICP-EOS) (ICPE-900, Shimadzu, Japan) was performed to measure the total concentration of iron dissolved during heterogeneous Fenton-like experiments [43]. An InoLab WTW pH-meter was used to monitor the pH of aqueous solutions.

3.3. Experimental Procedures

The chemical and photochemical experiments were carried out in the reactor equipped with a UV lamp (Heraeus Noblelight) (YNN 15/32, 125 W) mercury vapor, a magnetic stirrer, and a thermometer. The photo-reactor (pyrex) of 2 L capacity was placed in the first part. The lamp was located in an axial position submerged in a vertical immersion tube contained in a vertical cooling tube and immersed in the solution. Water was circulated between the lamp and glass vessel. The experience was mounted on a magnetic stirrer. In this work, only mercury vapor lamps that emit irradiation primarily to about 254 nm coincide with the absorption of our reagent which is H_2O_2. The volume of NA wastewater was 1 L. The pH of the solution was adjusted to the desired values by the addition of sodium hydroxide or sulfuric acid. After pH adjustment, a given weight of Fe_3O_4 was added. The magnetite was mixed very well with the solution of NA wastewater to form a homogeneous suspension. After the light of the lamp, a precise amount of hydrogen peroxide, 30%, was mixed with the suspension formed. At certain time intervals, samples of 10 mL volume were taken from the solution. The reaction was quenched with Na_2SO_3 and then analyzed

immediately to determine pH. The samples were filtered through 0.45 μm membrane filters and analyzed for inorganic ions, TOC, target compounds and intermediates, and UV-vis absorbance at wavelength (λ = 260 nm).

4. Conclusions

Natural iron mineral ore was successfully used as a heterogeneous catalyst for the decomposition of hydrogen peroxide into hydroxyl radicals in a Fenton-like process. The natural mineral ore was rich in α-Fe_2O_3 phase with the presence of Fe_3O_4 impurities. The decomposition of H_2O_2 by the natural Fe-based catalyst follows pseudo-first order kinetics. The formation of hydroxyl radicals was confirmed by the hydroxylation of benzoic acid to form salicylic acid. A Fe-based catalyst/H_2O_2 system was applied for the degradation of riluzole in water. A more rapid and highly efficient degradation of riluzole was obtained for catalyst particle sizes less than 200 μm of the natural Fe-based catalyst. The smaller the particle size of the catalyst, the larger its surface area and the greater its catalytic activity towards H_2O_2 decomposition into hydroxyl radicals. The degradation of riluzole can occur at all pH levels in the range 3.0–12.0 with a rate and efficiency greater than H_2O_2 oxidation alone, indicating that the natural Fe-based catalyst can function at any pH without the need to control the pH by the addition of chemicals. Higher concentrations of dissolved iron were measured at pH 12.0 and 3.0, while the lowest concentration of dissolved iron was measured at pH = 7.0. The final concentrations of dissolved iron measured in all pH values was less than 5 mg/L (<4% of the total iron contained in the catalyst composition). The increase of H_2O_2 concentration from 250 to 2000 mg/L increased the efficiency of riluzole degradation, while H_2O_2 concentrations higher than 1000 mg/L did not lead to an important enhancement in the efficiency and kinetics of riluzole degradation. An improvement in the efficiency and kinetics of the degradation of riluzole was observed under UV irradiation for both homogeneous and heterogeneous Fenton systems. UV irradiation enhances also the TOC removal for homogeneous and heterogeneous Fenton systems. The results of TOC and HPLC analysis demonstrate that the degradation of riluzole starts by the opening of the triazole ring to form aromatic derivatives including 4-TFMA, aniline, and 4-aminophenol releasing nitrate, sulfate, and fluoride ions. Successive oxidation stages transform the aromatic intermediates into C4 carboxylic acids that are quickly split into C2 carboxylic acids, which are slowly oxidized into CO_2 and H_2O. The reuse of the catalyst after heat treatment at 500 °C for 120 min and acid washing demonstrated that the heat-treated catalyst retained an efficiency >90% after five cycles; whereas the efficiency of the acid-treated catalyst dropped from one cycle to another to reach 62.4% after five cycles. The major advantage of the heterogeneous Fe-based catalyst/H_2O_2 system over homogeneous Fe^{2+}/H_2O_2 is the stability or reusability of the catalyst. The results revealed that the natural sources of iron, as a heterogeneous catalyst in Fenton-like system, are an appropriate replacement of a Fe^{2+} homogeneous catalyst that causes a secondary environmental problem in Fenton system applications. In addition, the reuse of the heat-treated heterogeneous catalyst represents an additional advantage of using natural iron-based catalyst in Fenton-like systems.

Author Contributions: Conceptualization: N.B. and A.B.; methodology: N.B. and M.I.A.; validation: N.B., A.B. and M.I.A.; formal analysis: E.N. and M.I.A.; investigation: E.N., A.B. and M.I.A.; resources: N.B.; data curation: E.N. and M.I.A.; writing—original draft preparation: N.B. and E.N.; writing—review and editing: N.B.; supervision: N.B. and A.B.; project administration: N.B. and M.I.A. All authors have read and agreed to the published version of the manuscript.

Funding: This research received no external funding.

Data Availability Statement: Not applicable.

Acknowledgments: The authors wish to acknowledge the Central Laboratories Unit (CLU), and the Center for Advanced Materials (CAM) at Qatar University for providing the spectroscopy and microscopy analysis.

Conflicts of Interest: The authors declare no conflict of interest.

References

1. Liu, R.; Dong, X.; Wang, X.C.; Zhang, P.; Liu, M.; Zhang, Y. Study on the Relationship among the Urbanization Process, Ecosystem Services and Human Well-Being in an Arid Region in the Context of Carbon Flow: Taking the Manas River Basin as an Example. *Ecol. Indic.* **2021**, *132*, 108248. [CrossRef]
2. Dong, H.; Xue, M.; Xiao, Y.; Liu, Y. Do Carbon Emissions Impact the Health of Residents? Considering China's Industrialization and Urbanization. *Sci. Total Environ.* **2021**, *758*, 143688. [CrossRef] [PubMed]
3. Doetterl, S.; Berhe, A.A.; Nadeu, E.; Wang, Z.; Sommer, M.; Fiener, P. Erosion, Deposition and Soil Carbon: A Review of Process-Level Controls, Experimental Tools and Models to Address C Cycling in Dynamic Landscapes. *Earth-Sci. Rev.* **2016**, *154*, 102–122. [CrossRef]
4. Regnier, P.; Friedlingstein, P.; Ciais, P.; Mackenzie, F.T.; Gruber, N.; Janssens, I.A.; Laruelle, G.G.; Lauerwald, R.; Luyssaert, S.; Andersson, A.J.; et al. Anthropogenic Perturbation of the Carbon Fluxes from Land to Ocean. *Nat. Geosci.* **2013**, *6*, 597–607. [CrossRef]
5. Jekel, M.; Ruhl, A.S.; Meinel, F.; Zietzschmann, F.; Lima, S.P.; Baur, N.; Wenzel, M.; Gnirß, R.; Sperlich, A.; Dünnbier, U.; et al. Anthropogenic Organic Micro-Pollutants and Pathogens in the Urban Water Cycle: Assessment, Barriers and Risk Communication (ASKURIS). *Environ. Sci. Eur.* **2013**, *25*, 20. [CrossRef]
6. Bueno, M.J.M.; Gomez, M.J.; Herrera, S.; Hernando, M.D.; Agüera, A.; Fernández-Alba, A.R. Occurrence and Persistence of Organic Emerging Contaminants and Priority Pollutants in Five Sewage Treatment Plants of Spain: Two Years Pilot Survey Monitoring. *Environ. Pollut.* **2012**, *164*, 267–273. [CrossRef]
7. Khan, S.; Naushad, M.; Govarthanan, M.; Iqbal, J.; Alfadul, S.M. Emerging Contaminants of High Concern for the Environment: Current Trends and Future Research. *Environ. Res.* **2022**, *207*, 112609. [CrossRef]
8. Ren, H.; Tröger, R.; Ahrens, L.; Wiberg, K.; Yin, D. Screening of Organic Micropollutants in Raw and Drinking Water in the Yangtze River Delta, China. *Environ. Sci. Eur.* **2020**, *32*, 67. [CrossRef]
9. Grandclément, C.; Seyssiecq, I.; Piram, A.; Wong-Wah-Chung, P.; Vanot, G.; Tiliacos, N.; Roche, N.; Doumenq, P. From the Conventional Biological Wastewater Treatment to Hybrid Processes, the Evaluation of Organic Micropollutant Removal: A Review. *Water Res.* **2017**, *111*, 297–317. [CrossRef]
10. Ghatak, H.R. Advanced Oxidation Processes for the Treatment of Biorecalcitrant Organics in Wastewater. *Crit. Rev. Environ. Sci. Technol.* **2014**, *44*, 1167–1219. [CrossRef]
11. Miklos, D.B.; Remy, C.; Jekel, M.; Linden, K.G.; Drewes, J.E.; Hübner, U. Evaluation of Advanced Oxidation Processes for Water and Wastewater Treatment–A Critical Review. *Water Res.* **2018**, *139*, 118–131. [CrossRef]
12. Deng, Y.; Zhao, R. Advanced Oxidation Processes (AOPs) in Wastewater Treatment. *Curr. Pollut. Rep.* **2015**, *1*, 167–176. [CrossRef]
13. Cheng, M.; Zeng, G.; Huang, D.; Lai, C.; Xu, P.; Zhang, C.; Liu, Y. Hydroxyl Radicals Based Advanced Oxidation Processes (AOPs) for Remediation of Soils Contaminated with Organic Compounds: A Review. *Chem. Eng. J.* **2016**, *284*, 582–598. [CrossRef]
14. Moreira, F.C.; Boaventura, R.A.R.; Brillas, E.; Vilar, V.J.P. Electrochemical Advanced Oxidation Processes: A Review on Their Application to Synthetic and Real Wastewaters. *Appl. Catal. B Environ.* **2017**, *202*, 217–261. [CrossRef]
15. Gągol, M.; Przyjazny, A.; Boczkaj, G. Wastewater Treatment by Means of Advanced Oxidation Processes Based on Cavitation–A Review. *Chem. Eng. J.* **2018**, *338*, 559–627. [CrossRef]
16. Aljuboury, A.; Palaniandy, P.; Bin, H.; Aziz, A. A Review on the Fenton Process for Wastewater Treatment. *J. Innov. Eng.* **2014**, *2*, 557–572. [CrossRef]
17. Pham, A.L.T.; Doyle, F.M.; Sedlak, D.L. Kinetics and Efficiency of H_2O_2 Activation by Iron-Containing Minerals and Aquifer Materials. *Water Res.* **2012**, *46*, 6454–6462. [CrossRef]
18. Badmus, K.O.; Tijani, J.O.; Massima, E.; Petrik, L. Treatment of Persistent Organic Pollutants in Wastewater Using Hydrodynamic Cavitation in Synergy with Advanced Oxidation Process. *Environ. Sci. Pollut. Res.* **2018**, *25*, 7299–7314. [CrossRef]
19. Pignatello, J.J.; Oliveros, E.; MacKay, A. Advanced Oxidation Processes for Organic Contaminant Destruction Based on the Fenton Reaction and Related Chemistry. *Crit. Rev. Environ. Sci. Technol.* **2006**, *36*, 1–84. [CrossRef]
20. Jain, B.; Singh, A.K.; Kim, H.; Lichtfouse, E.; Sharma, V.K. Treatment of Organic Pollutants by Homogeneous and Heterogeneous Fenton Reaction Processes. *Environ. Chem. Lett.* **2018**, *16*, 947–967. [CrossRef]
21. Mirzaei, A.; Chen, Z.; Haghighat, F.; Yerushalmi, L. Removal of Pharmaceuticals from Water by Homo/Heterogonous Fenton-Type Processes–A Review. *Chemosphere* **2017**, *174*, 665–688. [CrossRef] [PubMed]
22. Yaghmaeian, K.; Yousefi, N.; Bagheri, A.; Mahvi, A.H.; Nabizadeh, R.; Dehghani, M.H.; Fekri, R.; Akbari-adergani, B. Combination of Advanced Nano-Fenton Process and Sonication for Destruction of Diclofenac and Variables Optimization Using Response Surface Method. *Sci. Rep.* **2022**, *12*, 20954. [CrossRef] [PubMed]
23. Elwakeel, K.Z.; El-Bindary, A.A.; Kouta, E.Y. Retention of Copper, Cadmium and Lead from Water by Na-Y-Zeolite Confined in Methyl Methacrylate Shell. *J. Environ. Chem. Eng.* **2017**, *5*, 3698–3710. [CrossRef]
24. Kiwaan, H.A.; Atwee, T.M.; Azab, E.A.; El-Bindary, A.A. Efficient Photocatalytic Degradation of Acid Red 57 Using Synthesized ZnO Nanowires. *J. Chin. Chem. Soc.* **2019**, *66*, 89–98. [CrossRef]
25. Nadejde, C.; Neamtu, M.; Hodoroaba, V.-D.; Schneider, R.; Paul, A.; Ababei, G.; Panne, U. Green Fenton-like Catalysts for the Removal of Water Pollutants. In Materials for Energy, Efficiency and Sustainability. *J. Nanopart. Res.* **2015**, *17*, 476. [CrossRef]

26. Lima, M.J.; Silva, C.G.; Silva, A.M.T.; Lopes, J.C.B.; Dias, M.M.; Faria, J.L. Homogeneous and Heterogeneous Photo-Fenton Degradation of Antibiotics Using an Innovative Static Mixer Photoreactor. *Chem. Eng. J.* **2017**, *310*, 342–351. [CrossRef]
27. Srivastava, M.P.; Pan, S.K.; Prasad, N.; Mishra, B.K. Characterization and Processing of Iron Ore Fines of Kiruburu Deposit of India. *Int. J. Miner. Process.* **2001**, *61*, 93–107. [CrossRef]
28. Liu, Y.; Jin, W.; Zhao, Y.; Zhang, G.; Zhang, W. Enhanced Catalytic Degradation of Methylene Blue by A-Fe2O3/Graphene Oxide via Heterogeneous Photo-Fenton Reactions. *Appl. Catal. B Environ.* **2017**, *206*, 642–652. [CrossRef]
29. Kongsat, P.; Kudkaew, K.; Tangjai, J.; O'Rear, E.A.; Pongprayoon, T. Synthesis of Structure-Controlled Hematite Nanoparticles by a Surfactant-Assisted Hydrothermal Method and Property Analysis. *J. Phys. Chem. Solids* **2021**, *148*, 109685. [CrossRef]
30. Bensalah, N.; Dbira, S.; Bedoui, A. Mechanistic and Kinetic Studies of the Degradation of Diethyl Phthalate (DEP) by Homogeneous and Heterogeneous Fenton Oxidation. *Environ. Nanotechnol. Monit. Manag.* **2019**, *11*, 100224. [CrossRef]
31. Bensalah, N.; Ahmad, M.I.; Bedoui, A. Catalytic degradation of 4-ethylpyridine in water by heterogeneous photo-Fenton process. *Appl. Sci.* **2019**, *9*, 5073. [CrossRef]
32. Hussain, S.; Aneggi, E.; Goi, D. Catalytic Activity of Metals in Heterogeneous Fenton-like Oxidation of Wastewater Contaminants: A Review. *Environ. Chem. Lett.* **2021**, *19*, 2405–2424. [CrossRef]
33. Thomas, N.; Dionysiou, D.D.; Pillai, S.C. Heterogeneous Fenton Catalysts: A Review of Recent Advances. *J. Hazard. Mater.* **2021**, *404*, 124082. [CrossRef] [PubMed]
34. Benzaquén, T.B.; Barrera, D.A.; Carraro, P.M.; Sapag, K.; Alfano, O.M.; Eimer, G.A. Nanostructured Catalysts Applied to Degrade Atrazine in Aqueous Phase by Heterogeneous Photo-Fenton Process. *Environ. Sci. Pollut. Res.* **2019**, *26*, 4192–4201. [CrossRef]
35. Nidheesh, P.V. Heterogeneous Fenton Catalysts for the Abatement of Organic Pollutants from Aqueous Solution: A Review. *RSC Adv.* **2015**, *5*, 40552–40577. [CrossRef]
36. Gogoi, A.; Navgire, M.; Sarma, K.C.; Gogoi, P. Fe3O4-CeO2metal Oxide Nanocomposite as a Fenton-like Heterogeneous Catalyst for Degradation of Catechol. *Chem. Eng. J.* **2017**, *311*, 153–162. [CrossRef]
37. Oliveira, C.; Alves, A.; Madeira, L.M. Treatment of Water Networks (Waters and Deposits) Contaminated with Chlorfenvinphos by Oxidation with Fenton's Reagent. *Chem. Eng. J.* **2014**, *241*, 190–199. [CrossRef]
38. Muwanguzi, A.J.B.; Karasev, A.V.; Byaruhanga, J.K.; Jönsson, P.G. Characterization of Chemical Composition and Microstructure of Natural Iron Ore from Muko Deposits. *ISRN Mater. Sci.* **2012**, *2012*, 9. [CrossRef]
39. Das, S.K.; Kumar, S.; Ramachandrarao, P. Exploitation of Iron Ore Tailing for the Development of Ceramic Tiles. *Waste Manag.* **2000**, *20*, 725–729. [CrossRef]
40. Zhang, M.H.; Dong, H.; Zhao, L.; Wang, D.X.; Meng, D. A Review on Fenton Process for Organic Wastewater Treatment Based on Optimization Perspective. *Sci. Total Environ.* **2019**, *670*, 110–121. [CrossRef]
41. Raji, M.; Tahroudi, M.N.; Ye, F.; Dutta, J. Prediction of heterogeneous Fenton process in treatment of melanoidin-containing wastewater using data-based models. *J. Environ. Manag.* **2022**, *307*, 114518. [CrossRef] [PubMed]
42. Narapusetti, A.; Bethanabhatla, S.S.; Sockalingam, A.; Pilli, N.R.; Repaka, N.; Alla, T. Bioanalysis of Riluzole in Human Plasma by a Sensitive LC-MS/MS Method and Its Application to a Pharmacokinetic Study in South Indian Subjects. *Anal. Methods* **2014**, *6*, 4823–4830. [CrossRef]
43. Oral, E.V. ICP-OES Method for the Determination of Fe, Co, Mn, Cu, Pb, and Zn in Ore Samples from the Keban Region Using Experimental Design and Optimization Methodology. *At. Spectrosc.* **2016**, *37*, 142–149. [CrossRef]